Journal of Multidisciplinary Engineering Science and Technology (JMEST)
ISSN: 3159-0040
Vol. 2 Issue 5, May - 2015

Post-buckling Behavior of Elastic-Plastic Functionally Graded Beams Subjected to Eccentric Axial Load

Dinh-Kien Nguyen[1], Buntara S. Gan[2*], Thanh-Huong Trinh[2], S. Alexandrov[3]
[1]Institute of Mechanics, VAST, 18 Hoang Quoc Viet, Hanoi, Vietnam
[2]Department of Architecture, College of Engineering, Nihon University, Koriyama, Japan
[3]Laboratory of Fracture Mechanics, Institute for Problems in Mechanics, Moscow 11926, Russia
[2*] buntara@arch.ce.nihon-u.ac.jp

***Abstract*— This paper investigates the post-buckling behavior of elastic-plastic functionally graded (FG) beams subjected to an eccentric axial load by using the finite element method. The FG material is assumed to be formed from ceramic and metal with volume fractions varying in the thickness by a power-law function. Tamura-Tomota-Ozawa (TTO) model is used to evaluate the elastic-plastic properties of the beam material. A nonlinear finite element formulation is derived and used to construct the nonlinear equilibrium equations. An incremental-iterative procedure in combination with the arc-length method is employed in computing the load-displacement curves. Numerical results show that the post-buckling behavior of the beams plays an important role in the post-buckling behavior, and this deformation should be taken into consideration when studying the post-buckling behavior of the beams. A parametric study is carried out to highlight the effect of the volume fraction exponent and the eccentric ratio on the post-buckling behavior of the beams.**

Keywords—FG beam; elastic-plastic material; post-buckling behavior; eccentric axial load; finite element method

I. INTRODUCTION

Functionally graded (FG) materials have been drawn much attention from researchers since its first initiated by Japanese scientists in Sendai [1]. FG material is produced by gradually varying volume fraction of constituent materials, usually ceramic and metal, in a desired spatial direction. The effective properties of the resulted material exhibit continuous change, and thus eliminating interface problem and reducing stress concentration that often met in conventional composites. FG materials have promising application in aerospace, electronics, nuclear engineering and civil engineering [2, 3]. A large number of publications on the analysis of FG structures can be found in the literature, contributions that are most relevant to the topic of the present paper are briefly discussed below.

Chakraborty et al. [4] developed a shear deformation beam element for analyzing the thermo-elastic behavior of FG beams. Based on the third-order shear deformation beam element, Kadoli et al. [5] studied the static behavior of FG beams in ambient temperature. Kang and Li [6, 7] investigated the large displacements of FG beams subjected to a transverse end force or end moment. Nguyen [8, 9] derived the co-rotational beam elements for large displacement analysis of tapered axially and transversely FG beams. Also using the finite element method, Nguyen and Gan [10], Nguyen et al. [11] studied the geometrically nonlinear behavior of FG beam and frame structures.

Analysis of elastic-plastic FG structures has been drawn some attention from researchers in recent years. Gunes et al. [12] employed the finite element code LS-DYNA to study the elastic-plastic response of FG circular plates under low-velocity impact loads. Jahromi et al. [13] adopted a bilinear tress-strain model in studying the elastic-plastic behavior of an FG rotating disk. The stress field of the disk is computed with the aid of the finite element package ABAQUS. Huang and Han [14], Huang et al. [15] used a multi-linear hardening elastic-plastic material to study the elastic-plastic buckling of FG cylindrical shells under the axial and torsion loads, respectively. Also using the multi-linear hardening elastic-plastic material model, Zhang et al. [16] studied the buckling behavior of elastic-plastic FG cylindrical shells under a combination of the axial compressive load and external pressure. A detail examination on the effects of dimensional parameters and elastic-plastic material properties on the stability region and elastic-plastic interface of the shells has been given in [16] with the aid of Galerkin method.

In this paper, the post-buckling behavior of elastic-plastic FG beam subjected to an eccentric axial load is investigated by using the finite element method. The beam material is assumed to be formed from ceramic and metal with volume fraction varying in the thickness direction by a power-law function. The elastic-plastic properties of the beams are evaluated by Tamura-Tomota-Ozawa (TTO) model. A nonlinear finite element formulation based on Bernoulli beam theory is formulated by assuming a bilinear hardening stress-strain model for the elastic-plastic material. The formulation adopted the nonlinear von Kármán strain-displacement relationship is derived by using the neutral surface as reference plane. An incremental-iterative procedure in combination with the arc-length control method is employed in solving nonlinear equilibrium equations and computing the load-

displacement curves. The effect of the material exponent, the plastic deformation on the post-buckling behavior of the beam is investigated in detail. The influence of the eccentric ratio of the behavior of the beam is also examined and highlighted.

II. ELASTIC-PLASTIC FG BEAM

Fig. 1 shows a cantilever FG beam subjected to an eccentric axial load P. Denoting L, h, b are the length height and width of the beam, respectively. The beam material assumed to be formed from ceramic and metal in which volume fractions of constituent materials follow a simple power-law function as

$$V_c = \left(\frac{z}{h} + \frac{1}{2}\right)^n, V_c + V_m = 1 \quad (1)$$

where z is the transverse coordinate; V_c and V_m are respectively the volume fractions of ceramic and metal, and n is the volume fraction exponent. In Eq. (1) and hereafter, the subscripts 'c' and 'm' stand for 'ceramic' and 'metal', respectively.

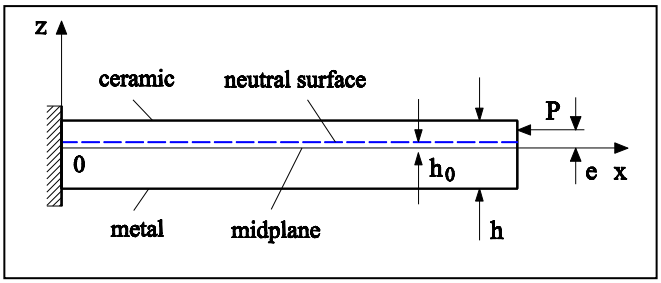

Fig. 1. *A cantilever FG beam under an eccentric axial load.*

The linear elastic behavior of FG material is described by Hook's law, and its effective material properties can be evaluated by micromechanics models used in conventional composites. The elastic-plastic behavior of ceramic/metal FG materials is widely described by using TTO model [17]. According to the TTO model, the uniaxial stress σ, and strain ε of a two-phase composite are related to the corresponding average uniaxial stresses and strains of the two constituent materials by [12, 13]

$$\sigma = \sigma_c V_c + \sigma_m V_m, \varepsilon = \varepsilon_c V_c + \varepsilon_m V_m \quad (2)$$

In the TTO model, an additional parameter q represented the ratio of stress to strain transfer is introduced as

$$q = \frac{\sigma_c - \sigma_m}{\varepsilon_c - \varepsilon_m}, 0 < q < \infty \quad (3)$$

The value of q depends on the properties of constituent materials and the micro-structural interaction in the composite.

In the TTO model for a ceramic/metal FGM, ceramic phase is assumed to be linearly elastic during its deformation process. Plastic deformation of the composite arose from plastic flow of the metal phase when the stress exceeds its yield limit. Here, a bilinear stress-strain relation with an isotropic hardening is assumed for the elastic-plastic behavior of metal. This model, as illustrated in Fig. 2 represents a constant tangent modulus E_{tm} when the stress in metal phase exceeds its yield limit σ_{Ym}. The elastic-plastic behavior of the ceramic/metal FG material also follows a bilinear isotropic hardening model represents a tangent modulus E_t in the plastic region (blue lines in Fig. 2).

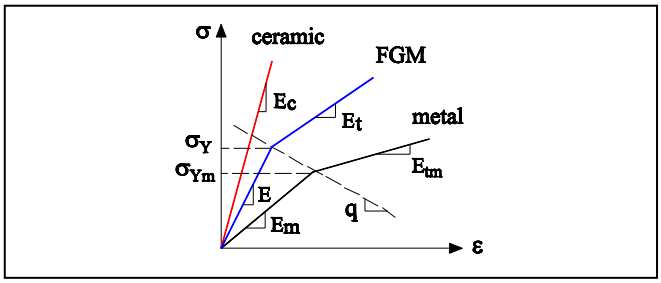

Fig. 2. *Bilinear elastic-plastic model for FG material.*

The effective properties such as Young's modulus E, yield stress σ_Y and tangent modulus E_t of the FG material are evaluated from the corresponding parameters of constituent materials and the parameter q by using TTO model as [12, 13]

$$E = \left[E_m V_m \frac{q+E_c}{q+E_m} + E_c V_c\right] / \left[V_m \frac{q+E_c}{q+E_m} + V_c\right] \quad (4)$$

$$\sigma_Y = \sigma_{Ym}\left[V_m + \frac{q+E_m}{q+E_c}\frac{E_c}{E_m} V_c\right] \quad (5)$$

$$E_t = \left[E_{tm} V_m \frac{q+E_c}{q+E_{tm}} + E_c V_c\right] / \left[V_m \frac{q+E_c}{q+E_m} + V_c\right] \quad (6)$$

The Young's modulus defined by Eq. (4) is, however not symmetrical with respect to the mid-plane, and thus the neutral surface is no longer coincident with the mid-plane. The shift of the neutral surface from the mid-plane, h_0 (see Fig. 1), is determined as [18]

$$h_0 = \int_{-h/2}^{h/2} E(z) z dz \,/\, \int_{-h/2}^{h/2} E(z) dz \quad (7)$$

It should be noted that with $E(z)$ given by Eq. (4), the integrals in the above equations cannot be evaluated explicitly. The Simpson rule is employed herein to evaluate the integrals and to determine h_0.

III. FINITE ELEMENT FORMULATION

This section derives the finite element formulation for the buckling analysis of the FG beam. Adopting the neutral surface as reference plane, the axial and transverse displacements at any point according to Euler-Bernoulli beam theory are as follows

$$u_1 = u - (z - h_0) w_{,x}, u_3 = w(x) \quad (8)$$

where u_1 and u_3 are the displacements at any point in directions of the x- and z-axes, and a subscript comma is used to indicate the derivative with respect the followed parameter.

A degenerated form of Green strain can be adopted for the buckling analysis as [19]

$$\varepsilon = u_{,x} + 0.5 w_{,x} + (z - h_0)\chi = \varepsilon_0 + (z - h_0)\chi \quad (9)$$

where $\varepsilon_0 = u_{,x} + 0.5 w_{,x}$ is the membrane strain, and $\chi = -w_{,xx}$ is the beam curvature.

The incremental stress-strain relationship for the one-dimensional elastic-plastic analysis can be written in the form [20]

$$d\sigma = E_{ep} d\varepsilon \tag{10}$$

where E_{ep} is the instantaneous modulus, and for the bilinear model adopted herein it has followed the simple form

$$E_{ep} = \frac{d\sigma}{d\varepsilon} = \begin{cases} E \text{ if } \sigma \le \sigma_Y \\ E_t \text{ if } \sigma > \sigma_Y \end{cases} \tag{11}$$

with σ_Y and E_t are the yield stress and tangent modulus of the FG material, respectively.

Assuming the beam is being divided into a number of two-node beam elements with a length of *l*. The vector of nodal displacements for a generic element has six degrees of freedom as

$$\boldsymbol{d} = \{u_1\ w_1\ \theta_1\ \ u_2\ w_2\ \theta_2\}^T \tag{12}$$

where u_i, w_i and θ_1 (i=1, 2) are axial and transverse displacements and rotation at node *i*. In Eq. (12) and hereafter, a superscript '*T*' is used to designate the transpose of a vector or a matrix.

The displacements between the two nodes of the element are interpolated from the nodal displacements according to

$$u = \boldsymbol{N}_u^T \boldsymbol{u}\ , w = \boldsymbol{N}_w^T \boldsymbol{w} \tag{13}$$

where $\boldsymbol{N}_u$=$\{N_{u1}\ \ N_{u2}\ \}^T$ is the matrix of shape functions for *u*, and $\boldsymbol{N}_w$=$\{N_{w1}\ N_{w2}\ N_{w3}\ N_{w4}\}^T$ is the matrix of shape functions for *w* . The following linear and cubic Hermite polynomials are adopted for N_{ui} (i=1, 2) and N_{wj} (j=1.4)

$$N_{u1} = \frac{l-x}{l}\ , N_{u2} = \frac{x}{l} \tag{14}$$

and

$$\begin{cases} N_{w1} = 1 - 3\frac{x^2}{l^2} + \ 2\frac{x^3}{l^3}, N_{w2} = x - 2\frac{x^2}{l} + \frac{x^3}{l^2} \\ \ \ N_{w3} = -3\frac{x^2}{l^2} - \ 2\frac{x^3}{l^3}\ , N_{w4} = -2\frac{x^2}{l} + \frac{x^3}{l^2} \end{cases} \tag{15}$$

In Eq. (13), we used the following notations

$$\boldsymbol{u} = \{u_1\ u_2\}^T, \boldsymbol{w}\ = \{\ w_1\ \theta_1\ w_2\ \theta_2\}^T \tag{16}$$

The finite element formulation based on the normal strain (8) and the shape functions (13) and (14), however, encounters the membrane locking [19]. In order to overcome this problem, the membrane strain $\boldsymbol{\varepsilon}_0$ in Eq. (9) should be replaced by an average strain, ε_{av}, defined as [19]

$$\varepsilon_{av} = \frac{1}{\mathrm{l}}\int_0^{\mathrm{l}} \varepsilon_0 dx\ = \frac{1}{\mathrm{l}}\int_0^{\mathrm{l}} \left(u_{,x} + 0.5 w_{,x}^2\right) dx \tag{17}$$

Substituting Eqs. (14) and (15) into Eq. (17) one gets

$$\varepsilon_{av} = \frac{1}{\mathrm{l}}(u_2 - u_1) + \frac{1}{30\mathrm{l}^2}[3\mathrm{l}(w_1 - w_2)(\theta_1 + \theta_2)$$
$$+18(w_1 - w_2)^2 + \mathrm{l}^2(2\theta_1^2 - \theta_1\theta_2 + 2\theta_2^2)] \tag{18}$$

The normal strain ε can be now written in the form

$$\varepsilon = \boldsymbol{b}_u^T \boldsymbol{u} + \frac{1}{2\mathrm{l}} \boldsymbol{w}^T \int_0^{\mathrm{l}} \boldsymbol{b}_w \boldsymbol{b}_w^T dx\ \boldsymbol{w} + (z - h_0)\boldsymbol{w}_w^T \boldsymbol{w} \tag{19}$$

and

$$\boldsymbol{b}_u = \frac{d\boldsymbol{N}_u}{dx}\ , \boldsymbol{b}_w = \frac{d\boldsymbol{N}_w}{dx}\ , \boldsymbol{c}_w = \frac{\mathrm{d}^2\boldsymbol{N}_w}{dx^2} \tag{20}$$

The virtual strain δU for the element is given by

$$\delta U = \int_V \ \sigma \delta\varepsilon\ dV \tag{21}$$

where *V* is the element volume; σ is the normal stress, and $\boldsymbol{\delta\varepsilon}$ is the virtual normal strain that can be computed from Eqs. (17) and (18) as

$$\delta\varepsilon = \boldsymbol{b}_u^T \delta\boldsymbol{u} + [\boldsymbol{e}_w^T + (z - h_0)\boldsymbol{c}_w^T]\delta\boldsymbol{w} \tag{22}$$

where $\boldsymbol{e}_w$ is obtained from Eq. (18) as follows

$$\boldsymbol{e}_w = \frac{d\varepsilon_{av}}{d\boldsymbol{w}} = \begin{Bmatrix} \frac{1}{10l}[12(w_1 - w_2) + l(\theta_1 + \theta_2)] \\ \frac{1}{30}[3(w_1 - w_2) + l(4\theta_1 - \theta_2)] \\ \frac{1}{10l}[12(w_2 - w_1) + l(\theta_1 + \theta_2)] \\ \frac{1}{30}[3(w_2 - w_1) + l(4\theta_2 - \theta_1)] \end{Bmatrix} \tag{23}$$

Substituting Eq. (22) into Eq. (21) one can obtain the element nodal forces in the forms

$$\boldsymbol{f}_u = \{N_1\ N_2\}^T\ = \int_{\boldsymbol{V}} \ \boldsymbol{b}_u \sigma dV \tag{24}$$

and

$$\boldsymbol{f}_w = \{M_1\ Q_1\ M_2\ Q_2\}^T = \int_{\boldsymbol{V}} \ [\boldsymbol{e}_w + (z - h_0)\boldsymbol{e}_w]\sigma dV \tag{25}$$

In Eqs. (24) and (25), $\boldsymbol{f}_u$ and $\boldsymbol{f}_w$ are the nodal force vectors corresponding to the axial and bending nodal displacements, respectively.

Finally, the tangent stiffness matrix $\boldsymbol{k}_t$ is obtained by differentiating the nodal forces with respect to the nodal displacements. For the sake of convenience, we split the tangent stiffness matrix into sub-matrices as

$$\boldsymbol{k}_t = \begin{bmatrix} \boldsymbol{k}_{uu} & \boldsymbol{k}_{uw} \\ \boldsymbol{k}_{wu} & \boldsymbol{k}_{ww} \end{bmatrix} \tag{26}$$

in which the $\boldsymbol{k}_{uu}$ and $\boldsymbol{k}_{ww}$ are the stiffness matrices stemming from element stretching and bending, respectively; $\boldsymbol{k}_{uw}$= $\boldsymbol{k}_{wu}{}^T$ is the stiffness resulted from the stretching-bending coupling. The expressions for these sub-matrices are as follows

$$\boldsymbol{k}_{uu} = \frac{d\boldsymbol{f}_u}{d\boldsymbol{u}} = \int_V \ \boldsymbol{b}_u E_{ep} \boldsymbol{b}_u^T dV \tag{27}$$

$$\boldsymbol{k}_{uw} = \frac{d\boldsymbol{f}_u}{d\boldsymbol{w}} = \int_V \ \boldsymbol{b}_u [\boldsymbol{e}_w^T + (z - h_0)\boldsymbol{c}_w^T] dV \tag{28}$$

and

$$\boldsymbol{k}_{ww} = \int_V \ \{[\boldsymbol{e}_w \boldsymbol{e}_w^T + (z - h_0)^2 \boldsymbol{c}_w \boldsymbol{c}_w^T] E_{ep+} \boldsymbol{A}\sigma\} dV \tag{29}$$

where $\boldsymbol{A}$ is a symmetrical matrix with the following form

$$\boldsymbol{A} = \frac{1}{30\mathrm{l}} \begin{bmatrix} 36 & 3\mathrm{l} & -36 & 3\mathrm{l} \\ 3\mathrm{l} & 4\mathrm{l}^2 & -3\mathrm{l} & -\mathrm{l}^2 \\ -36 & -3\mathrm{l} & 36 & -3\mathrm{l} \\ 3\mathrm{l} & -\mathrm{l}^2 & -3\mathrm{l} & 4\mathrm{l}^2 \end{bmatrix} \tag{30}$$

For the FG beam considered in this paper, both the yield stress σ_Y and tangent modulus E_t are functions of the transverse coordinate z, and thus the integrals in Eqs. (24)-(29) are not able to compute explicitly. Gauss quadrature with 7 points along the element length and 11 point through the beam thickness is employed herein to compute the integrals. In addition, a simple elastic-plastic algorithm for the one-dimensional problem described in Ref. [20] is used to update the normal stress and to compute the element formulation. The algorithm accounting for the hardening material requires storing the normal strain, yield stress, at the Gauss points. It should be noted that for homogeneous beams, the Young's modulus, tangent modulus and yield stress are constant, and the present formulation deduces to the beam element previous derived by the first three authors in Ref. [21].

Based on the derived finite element formulation, the nonlinear equilibrium equation for the beam can be written in the form [19]

$$\boldsymbol{g}(\boldsymbol{p},\lambda) = \boldsymbol{q}_{in}(\boldsymbol{p}) - \lambda \boldsymbol{f}_{ef} = \boldsymbol{0} \qquad (30)$$

where the out-of-balance force vector $\boldsymbol{g}$ is a function of the current global nodal displacements $\boldsymbol{p}$ and external loading parameter λ; $\boldsymbol{q}_{in}$ is the global vector of nodal forces, constructed by assembling the element nodal force vector; $\boldsymbol{f}_{ef}$ is the fixed external loading vector. Since the eccentric load P in Fig. 1 is statically equivalent to a centric load P acting on the neutral surface at the beam end plus a moment $M=Pe$, with e is the distance from the load to the neutral surface. The system of Eq. (30) can be solved by an incremental-iterative method, in which a new iterative displacement vector dp can be obtained from a truncated Taylor expansion of $\boldsymbol{g}(\boldsymbol{p},\lambda)$ around an equilibrium point ($\boldsymbol{p}_0$, λ_0 $\boldsymbol{f}_{ef}$) as

$$\boldsymbol{g}(\boldsymbol{p},\lambda) = \boldsymbol{g}_0 + \frac{d\boldsymbol{g}}{d\boldsymbol{p}}\Big|_0 \Delta\boldsymbol{p} = \boldsymbol{g}_0 + \boldsymbol{K}_t\Big|_0 \Delta\boldsymbol{p} = \boldsymbol{0} \qquad (31)$$

So that

$$\Delta\boldsymbol{p} = -\boldsymbol{K}_t^{-1}\Big|_0 \boldsymbol{g}_0 \qquad (32)$$

In the above equations, $\boldsymbol{K}_t$ is the global tangent stiffness matrix, obtain by assembling the above-derived element tangent stiffness $\boldsymbol{k}_t$ by the standard way of the finite element method. The notation '$|_0$' means that the stiffness matrix is evaluated at the equilibrium point ($\boldsymbol{p}_0$,λ_0 $\boldsymbol{f}_{ef}$). In order to trace a complete load-displacement curves in the post-buckling region, the arc-length method was adopted where Eq. (30) is augmented by a constraint equation. Details of the arc-length method and its implementation are described by Crisfield in Ref. [19].

IV. NUMERICAL RESULTS

The derived finite element formulation and described numerical algorithm were implemented into a computer code for investigating the post-buckling behavior of the FG beams. The numerical result reported in this section has been performed for FG beam with length L=5m, height h=0.1m and width b=0.2m. The properties of the constituent materials are adopted from Ref. [13] as follow: E_c=80 GPa for ceramic, E_m= 56 GPa, σ_{Ym}= 106 MPa, E_{tm}= 12 GPa for metal, and q=17.2 GPa. Figs. 3 and 4 show the variation of the Young's modulus and the yield stress in the thickness direction of the FG beam, respectively.

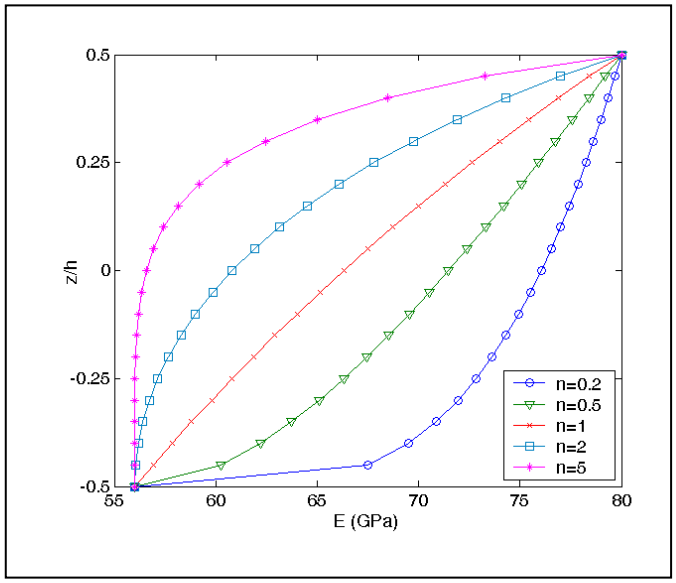

Fig. 3. *Variation of Young's modulus in thickness of FG beam*

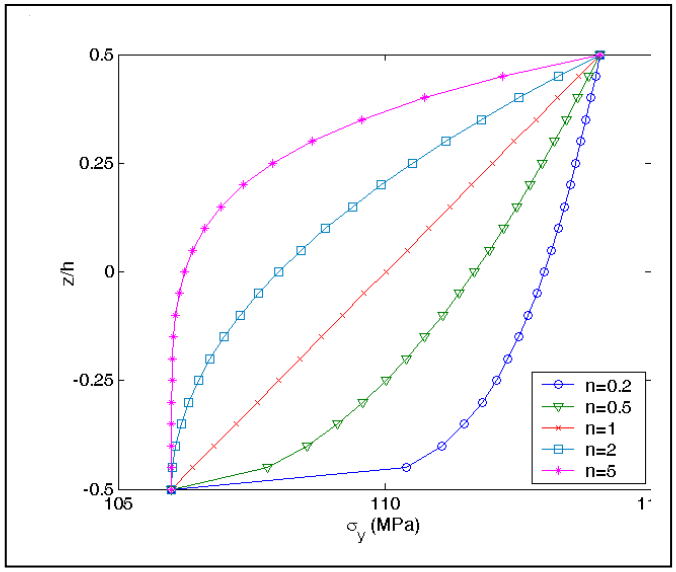

Fig. 4. *Variation of yield stress in thickness of FG beam*

Two kinds of boundary condition, namely clamped-free (CF) and simply supported (SS) are considered herein. Ten elements have been used to discrete the beam. Since the present formulation deduces to the one in [31] for homogeneous beam and to a special case of FG beam in [9], the accuracy and convergence of the formulation thus are confirmed.

Fig. 5 shows the load-displacement curves of the CF beam for various values of the volume fraction exponent n and an eccentric ratio ec/r^2= 0.005. In the figure, the deflection w is computed at the free end, and the applied load was normalized by the Euler

buckling load of homogeneous metal cantilever beam, that is $P_0= \pi^2 E_m I/4L^2$. The eccentric ratio, ec/r^2 (with r is the radius of gyration) is defined according to Ref. [22], but c is now measured from the top surface to the neutral surface, and thus $c=h/2-h_0$. As seen from the figure, similar to the homogeneous beam [21], the post-buckling of the beam is greatly affected by the plastic deformation, and post-buckling of the beam become unstable when the effect of plastic deformation is taken into consideration. The volume fraction exponent n alters the limit load of the beam, but it hardly affects the post-buckling behavior of the beam. It should be noted that the elastic curve in the figure was obtained by setting the yield stress σ_Y in the computer code to a large value so the yielding will not occur.

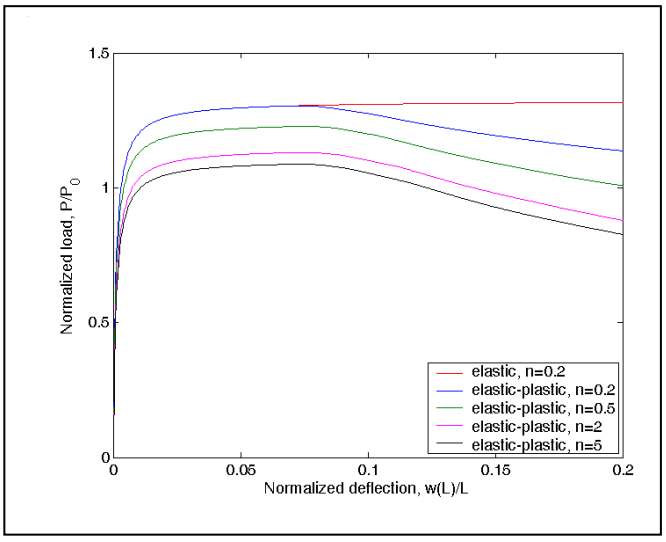

Fig. 5. *Load-displacement curves for CF beam with various values of exponent n (ec/r^2=0.005).*

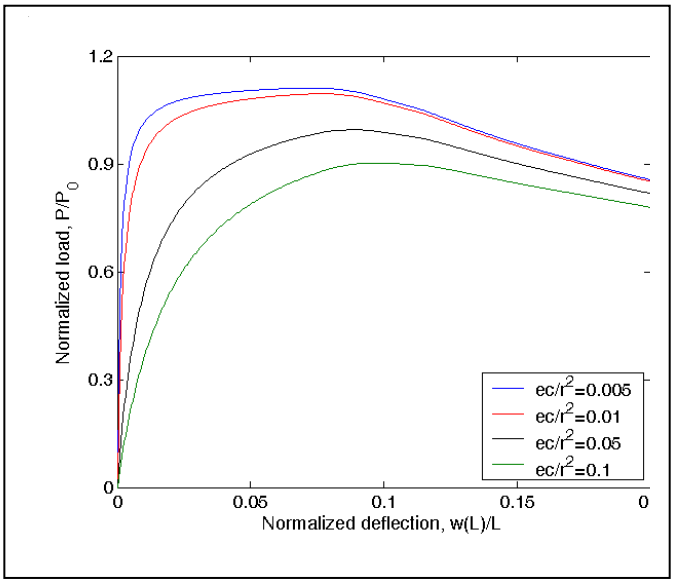

Fig. 6. *Effect of eccentric ratio on the post-buckling behavior of CF beam (n=3).*

The effect of the eccentric ratio on the post-buckling behavior of the CF beam is depicted in Fig. 6 for a value of a volume fraction exponent n=3. As seen from the figure, the post-buckling behavior of the beam is very sensitive to the eccentric ratio, and the limit load gradually reduces when increasing the eccentric ratio. This phenomenon is similar to the post-buckling behavior of the homogeneous elastic-plastic beams subjected to an axial load [21].

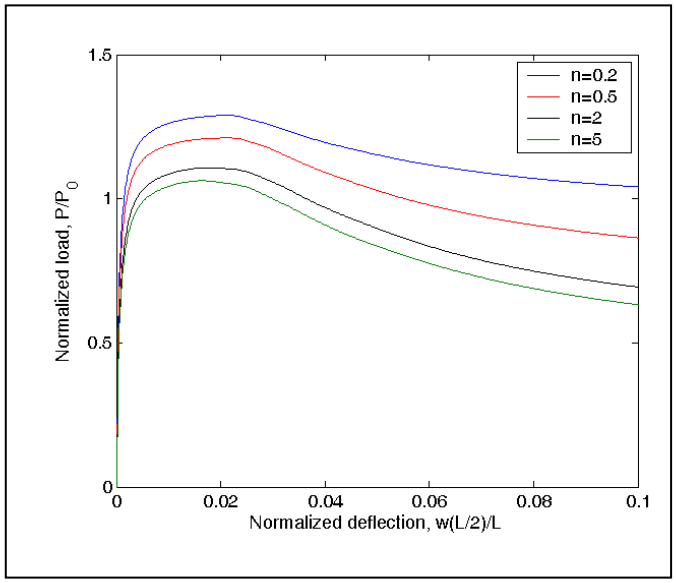

Fig. 7. *Load-displacement curves for SS beam with various values of exponent n (ec/r^2=0.005).).*

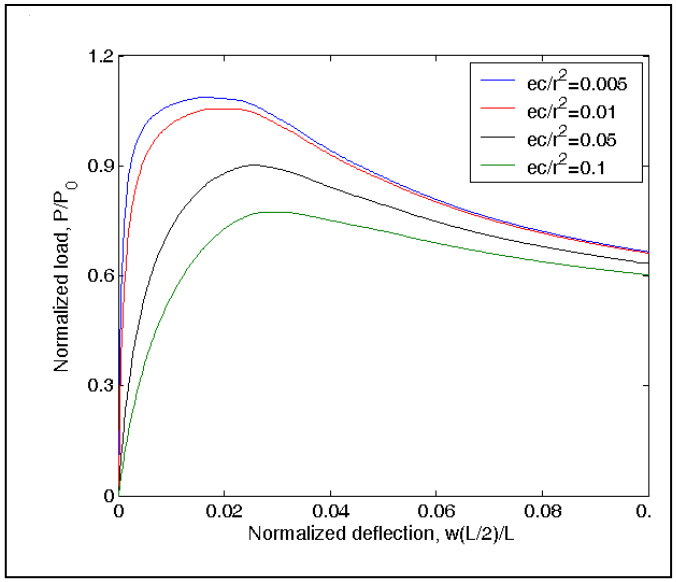

Fig. 8. *Effect of eccentric ratio on the post-buckling behavior of SS beam (n=3).*

In Fig. 7 the load-displacement curves of the SS beam are illustrated for various values of the volume fraction exponent n and an eccentric ratio ec/r^2= 0.005. In the figure, P_0 is the buckling load of simply supported metal beam, that is $P_0= \pi^2 E_m I/L^2$. As in the case of the CF beam, the volume fraction exponent changes the limit load of the beam, and the limit load reduces when increase the volume fraction exponent n. In addition, the post-buckling strength of the beam in the post-buckling region, measured in term of the ratio of applied load to the critical load P_0 of the metal beam reduces, regardless of the exponent n. This means

that the post-buckling of the beam is unstable. The effect of the eccentric ratio to the post-buckling behavior of the SS beam as depicted in Fig. 8 is similar to the CF beam, and the limit load considerably reduces when increase the eccentric ratio.

V. CONCLUSIONS

A finite element formulation for investigating the post-buckling behavior of elastic-plastic FG beams has been formulated. The formulation based on Euler-Bernoulli beam theory was derived by using the neutral surface as reference plane. The TTO model was employed in evaluating the elastic-plastic properties of the beam material. Gauss quadrature was used in computing the nodal internal force vector and tangent stiffness matrix. The nonlinear equilibrium equations have been solved by an incremental-iterative procedure in combination with the arc-length control method. Numerical examples have been demonstrated for beams with clamped-free and simply supported end conditions. The numerical results show that the plastic deformation greatly affects the post-buckling behavior of the FG beams, in which the post-buckling of the beam is unstable when the effect of plastic deformation is taken into account. The study emphasizes that the plastic deformation must be taken into account when investigating the post-buckling behavior of the beam. The influence of the volume fraction distribution, eccentric ratio on the post-buckling behavior of the beams has also been numerically studied and highlighted.

ACKNOWLEDGMENT

The research described in this paper has been supported by the grants VAST.HTQT.NGA.07/14-15 (Vietnam) and RFBR-14-01-93000 (Russia).

REFERENCES

[1] M. Koizumi, FGM activities in Japan, Compos. PtB Eng., vol. 28, pp. 1-4, 1997.

[2] S. Suresh, A. Mortensen, Functionally graded materials, London: The Institute of Materials, IOM Communications Ltd., 1998.

[3] D.K. Jha, T. Kant, R.K. Singh, A critical review of recent research on functionally graded plates, Compos. Struct., vol. 96, pp. 833-849, 2013.

[4] A. Chakraborty, S. Gopalakrishnan, J.R. Reddy, A new beam finite element for the analysis of functionally graded materials, Int. J. Mech. Sci. vol. 45, pp. 519-539, 2003.

[5] R. Kadoli, K. Akhtar, N. Ganesan, Static analysis of functionally graded beams using higher order shear deformation beam theory, Appl. Math. Model., vol. 32, pp. 2509-2525, 2008.

[6] Y.A. Kang, X.F. Li, Bending of functionally graded cantilever beam with power- law nonlinearity subjected to an end force. Int. J. Non-Linear Mech. Vol. 44, pp. 696–703, 2009.

[7] Y.A. Kang, X.F. Li, Large deflection of a non-linear cantilever functionally graded beam, J. Reinf. Plast. Compos., vol. 29, pp. 1761–1774, 2010.

[8] D.K. Nguyen, Large displacement response of tapered cantilever beams made of axially functionally graded material, Compos. Pt B Eng. , vol. 55, pp. 298-305, 2013.

[9] D.K. Nguyen, Large displacement behaviour of tapered cantilever Euler-Bernoulli beams made of functionally graded material, Appl. Math. Comput., vol. 237, pp. 340-355, 2014.

[10] D.K . Nguyen, B.S. Gan, Large deflections of tapered functionally graded beams subjected to end forces, Appl. Math. Model., vol. 38, pp. 3054-3066, 2014.

[11] D.K. Nguyen, B.S. Gan, T.H. Trinh, Geometrically nonlinear analysis of planar beam and frame structures made of functionally graded material, Structural Engineering and Mechanics, vol. 49, pp. 727-743, 2014.

[12] R. Gunes, M. Aydin, M. Kemal Apalak, J.R. Reddy, The elasto-plastic impact analysis of functionally graded circular plates under low-velocities, Compos. Struct., vol. 93, pp. 860–869, 2011.

[13] B.H. Jahromi, H. Nayeb-Hashemi, A. Vaziri, Elasto-Plastic Stresses in a Functionally Graded Rotating Disk, J. Eng. Mater-T ASME, vol.134, 021004–-11, 2012.

[14] H. Huang, Q. Han, Elastoplastic buckling of axially loaded functionally graded material cylindrical shells, Compos. Struct., vol. 117, pp 135–42, 2014.

[15] H. Huang, B. Chen, Q. Han, Investigation on buckling behaviors of elastoplastic functionally graded cylindrical shells subjected to torsional loads, Compos. Struct., Vol. 118, pp. 234–240, 2014.

[16] Y. Zhang, H. Huang, Q. Han, Buckling of elastoplastic functionally graded cylindrical shells under combined compression and pressure, Compos. Pt B Eng., vol. 69, pp. 120–126, 2015.

[17] I. Tamura, Y. Tomota, H. Ozawa, Strength and ductility of Fe–Ni–C alloys composed of austenite and martensite with various strength. In: Proceedings of the Third International Conference on Strength of Metals and Alloys, vol. 1. Cambridge: Institute of Metals, pp. 611–615, 1973.

[18] D.-G. Zhang, Nonlinear bending analysis of FGM beams based on physical neutral surface and high order shear deformation theory, Compos. Struct., vol. 100, pp. 121-226, 2013.

[19] M.A. Crisfield, Non-linear finite element analysis of solids and structures, Volume 1: Essentials, John Wiley & Sons, Chichester, 1991.

[20] R.D. Cook, D.S. Malkus, M.E. Plesha, Concepts and applications of finite element analysis, John Wiley & Sons, New York, 1989.

[21] D.K. Nguyen, T.H. Trinh, B.S. Gan, Post-buckling response of elastic-plastic beam resting on an elastic foundation to eccentric axial load, The IES J. Pt A: Civil Struct. Eng., vol. 5, pp. 43-49, 2012.

[22] J.M. Gere, S. Timoshenko, Mechanics of Materials, 3rd edition, Chapman & Hall, London, 1991.